

# Fictitious Domain Method for Unsteady Problems: Application to Electromagnetic Scattering

Francis Collino\*<sup>†</sup>      Patrick Joly\*<sup>†</sup>      Florence Millot<sup>†</sup>

**CERFACS REPORT TR/EL/96/32**

## 1 Introduction

In recent years, solving time dependent problems of scattering by an obstacle has received considerable attention. Among the various techniques that have been studied, the finite difference method is one of the most attractive. This method uses a regular grid with an explicit scheme in time and hence is very efficient from the computational point of view. However its great disadvantage is that it creates numerical diffraction when the obstacle boundary does not fit the grid mesh (see Fig. 1).

---

\*INRIA, Domaine de Rocquencourt 78153 Le Chesnay

<sup>†</sup>CERFACS, 42 avenue G. Coriolis 31057 Toulouse

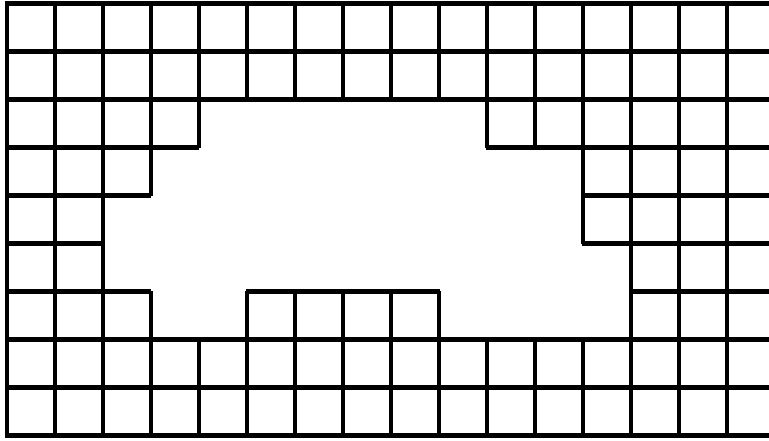


Fig 1: *Geometry of the problem*

A possibility for avoiding this drawback is to use a finite element method. The finite element mesh may follow exactly the boundary of the object (see Fig. 2).

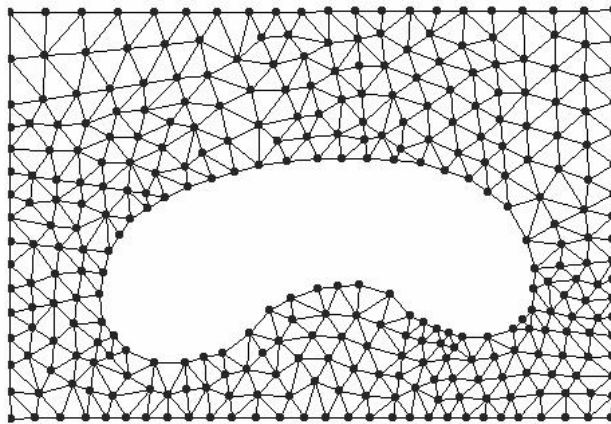


Fig 2: *Example of the conformous finite element mesh in 2D*

Nevertheless, other drawbacks are introduced. It appears necessary to use mass lumping to obtain an explicit scheme but this is still difficult to do in the case of higher order finite element methods ([6]), especially for Maxwell's equations. Furthermore, the numerical implementation is much more difficult and the efficiency of the computations is decreased by the unstructured nature of the data. Finally, meshing the boundary of the obstacle may induce meshes of small size and meshing the whole domain of computation with tetrahedrons is not an easy task. Moreover the time step has to be chosen in accordance with the

grid mesh size (C.F.L. condition), sometimes leading to small time steps.

In this paper, we investigate an alternative method for handling the scattering problem, namely, the fictitious domain method (noted the FDM). Such methods have recently been shown to have interesting potential for solving complicated problems ([1], [2], [3], [11], [14],[17]) particularly in the stationary case. The use of the FDM for time dependent problems is new [15]. It should reveal really efficiencies for those kinds of problems, particularly for exterior wave propagation problems such as for scattering by obstacles as we shall demonstrate in this paper. The FDM, also called the domain embedding method, consists in extending artificially the solution inside the obstacle so that the new domain of computation has a very simple shape (typically a rectangle in 2D). This extension requires the introduction of a new variable defined only at the boundary of the obstacle. This auxiliary variable accounts for the boundary condition; it can be related to a singularity across the boundary of the obstacle of the extended function. This idea will be developed in Section 2. The main point is that the mesh for the solution on the enlarged domain can be chosen independently of the geometry of the obstacle. In particular, the use of regular grids or structured meshes allows for simple and efficient computations. There is some additional computational cost due to the determination of the new boundary unknown. However, the final numerical scheme appears to be a slight perturbation of the scheme for the problem without an obstacle so this cost may be considered as marginal. Theoretically, the convergence of the method is linked to obtaining a uniform inf-sup condition which leads to a compatibility condition between the boundary mesh and the uniform mesh [13]. Another important point is that the stability condition of the resulting scheme is the same as the one of the finite difference scheme. Practically, it implies that the two mesh grids cannot be chosen completely independently, but this is not an important constraint.

The remainder of this article is divided into four sections. In Section 2, we introduce the

FDM for acoustic wave propagation with Dirichlet boundary conditions. We describe the formulation of the new problem, present the space and time discretization of this problem, and provide some remarks about error estimates. We also investigate the stability of the numerical scheme. In Section 3, we apply the method for the time dependent Maxwell equations, presenting a new formulation of the electromagnetic scattering problem. The space and time discretization are also discussed. Some numerical results are presented and discussed in Section 4. We show the superiority of the fictitious method in terms of accuracy and memory requirement over the method that consists in using a staircase like approximation of the boundary. This is confirmed by a very simple 1-D analysis which is presented in Section 5.

## 2 A fictitious domain method for an acoustic problem

### 2.1 Presentation of the method

We consider first the scattering of a wave by an obstacle  $\mathcal{O}$ ,  $\mathcal{O} \subset \mathbf{R}^d$  with  $d = 2$  or  $d = 3$ . The solution is governed by the wave equation in  $D$ , the open complement of the obstacle with a Dirichlet condition on the boundary:

$$\begin{cases} \frac{\partial^2 u}{\partial t^2} - \Delta u = 0 & \text{in } D \\ u = 0 & \text{on } \gamma = \partial D. \end{cases} \quad (1)$$

The incident wave is generated by initial conditions at time  $t = 0$  given by

$$u(x, 0) = u_0(x) \in \mathbf{H}^1(D), \quad \frac{\partial u}{\partial t}(x, 0) = u_1(x, 0) \in L^2(D). \quad (2)$$

In order to have a finite computational domain, the classical technique consists in bounding the domain  $D$  and in imposing absorbing conditions on the exterior boundary ([21], [10]).

For the sake of simplicity, a Dirichlet condition is assumed on the exterior boundary as well. For our purpose, we choose the geometry of the external boundary to be rectangular. We denote by  $\Omega$  this bounded domain and by  $C$  the rectangle  $\Omega \cup \mathcal{O}$ . We want to solve the simple problem described by

$$\begin{cases} \frac{\partial^2 u}{\partial t^2} - \Delta u = 0 & \text{in } \Omega \\ u = 0 & \text{on } \gamma \\ u = 0 & \text{on } \partial C, \end{cases} \quad (3)$$

by the FDM (see Fig. 3).

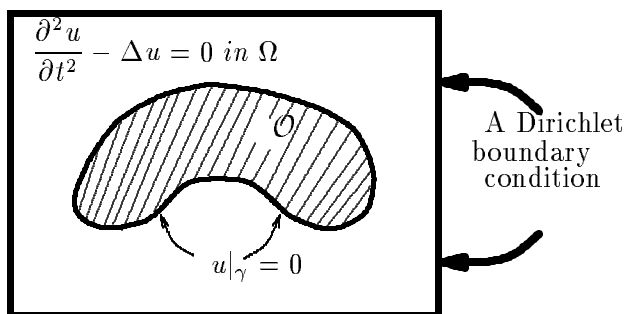


Fig 3: *Geometry of the problem*

### 2.1.1 Formulation of the new problem

The main idea of the FDM is to extend  $u$  from  $\Omega$  to the enlarged domain  $C$  to a function (still denoted by  $u$  for simplicity) with  $H^1(C)$  regularity. Note that this regularity requirement implies the continuity of the trace of  $u$  across the boundary.

More precisely, we look for  $u$  in the space

$$u \in \tilde{V} = \{v \in H^1(C); v = 0 \text{ on } \gamma\}, \quad (4)$$

and we define  $u$  as the first argument of  $(u, \lambda)$  the solution of the following variational

evolution problem

$$\begin{cases} \frac{d^2}{dt^2}(u, v) + a(u, v) = b(v, \lambda) & \forall v \in X \\ b(u, \mu) = 0 & \forall \mu \in M, \end{cases} \quad (5)$$

where  $X = H_0^1(C)$  and  $M = H^{-1/2}(\gamma)$ . We introduce  $H = L^2(C)$  so that  $X$  is densely and continuously embedded in  $H$  and denote by  $(\cdot, \cdot)$  the scalar product in  $H$

$$(u, v) = \int_C uv \, dx, \quad (6)$$

and the bilinear form  $a(u, v)$  by

$$a(u, v) = \int_C \nabla v \nabla u \, dx, \quad (7)$$

which is continuous and coercive in the space  $X$ . The bilinear form  $b(u, \mu)$  denotes the duality pairing between  $H^{-1/2}(\gamma)$  and  $H^{1/2}(\gamma)$  and is equal to

$$b(u, \mu) = \langle \mu, u \rangle_\gamma = \int_\gamma \mu u \, d\gamma. \quad (8)$$

We note by  $|\cdot|$ ,  $\|\cdot\|_X$  and  $\|\cdot\|_M$  the respective norms in  $H$ ,  $X$  and  $M$ . We have

$$|v| \leq \|v\|_X = \sqrt{|v|^2 + a(v, v)} \quad \forall v \in X. \quad (9)$$

In principle, the FDM consists in extending the solution in the enlarged computational domain and to introduce a new unknown at the boundary. The main difference between this approach and a standard conforming finite element approach lies in the fact that the Dirichlet condition is taken into account in a weak sense instead of being imposed in the functional space. It has a relationship with other approaches as we shall demonstrate in

the next two sections.

### 2.1.2 A justification of (5) via minimization problems

To understand (5), let us consider the time  $t$  as a parameter and the function  $f = -\frac{\partial^2 u}{\partial t^2}$  as a data. We then have to solve the following problem

$$\begin{cases} -\Delta u = f & \text{in } \Omega \\ u = 0 & \text{on } \gamma. \end{cases} \quad (10)$$

It is equivalent to minimize the functional  $J(v) = \int_C \left\{ \frac{1}{2} |\nabla v|^2 - fv \right\} dx$  over the set  $V$  of functions of  $H^1(\Omega)$  satisfying the constraint  $v = 0$  on  $\gamma$ . The functions belonging to  $V$  can be seen as the restrictions of functions of  $\tilde{V}$  defined in (4). It is natural to consider the enlarged minimization problem defined by

$$\min_{\tilde{v} \in \tilde{V}} J(\tilde{v}) = \int_C \left\{ \frac{1}{2} |\nabla \tilde{v}|^2 - \tilde{f} \tilde{v} \right\} dx, \quad (11)$$

where for instance  $\tilde{f} = 0$  on  $\mathcal{O}$  and  $\tilde{f} = f$  on  $\Omega$ . It is easy to verify that the restriction of the solution of problem (11) to  $\Omega$  is exactly the solution of problem (5) that we are looking for. Problem (5) is a minimization problem with an equality constraint. Its solution is the first argument of the saddle point of the Lagrangian functional defined by  $L(v, \mu) = J(v) - b(v, \mu)$ . Noting that the derivative of this Lagrangian is equal to zero at the optimum  $(u, \lambda)$ , we obtain:

$$\begin{cases} a(u, v) = b(v, \lambda) + (f, v) & \forall v \in X \\ b(u, \mu) = 0 & \forall \mu \in M, \end{cases} \quad (12)$$

which gives exactly the equations of (5) if we have written  $f = -\frac{\partial^2 u}{\partial t^2}$ .

Thus the auxiliary unknown  $\lambda$  of problem (5) appears as the associated Lagrange multiplier.

### 2.1.3 An analogy with integral equations methods

Another way to understand the system of equations (5) is to say that having extended  $u$  by continuity across  $\gamma$  and assuming that  $u$  still satisfies the wave equation inside  $\mathcal{O}$  (this means that  $u$  solves the homogeneous Dirichlet problem inside and outside), we have in the sense of distributions on  $C$

$$\frac{\partial^2 u}{\partial t^2} - \Delta u = \left[ \frac{\partial u}{\partial n} \right]_{\gamma} \delta_{\gamma}. \quad (13)$$

where  $\delta_{\gamma}$  is the surface measure supported on  $\gamma$ . Then, it is not difficult to reinterpret  $\lambda$  as being the jump of the normal derivative of  $u$  across  $\gamma$ . This establishes an analogy between the FDM and the integral equations for scattering problems [4]. Indeed, in this kind of method  $\lambda$  is typically the quantity that is chosen as the unknown. Nevertheless let us point out a very important difference between our approach and these methods. Integral equations are known to lead, after discretization, to the solution of full linear systems in  $\lambda$ ; as will be shown later, this will not be the case for the FDM.

## 2.2 Finite element approximation and time discretization

### 2.2.1 Space discretization

Let  $X_h$  (respectively  $M_h$ ) be a finite dimensional subspace of  $X$  (respectively  $H^{-1/2}(\gamma)$ ).

We approximate the variational problem (5) by

$$\left\{ \begin{array}{l} \text{Find } u_h \in X_h, \quad \lambda_h \in M_h \quad \text{such that} \\ \frac{d^2}{dt^2}(u_h, v_h) + a(u_h, v_h) = b(v_h, \lambda_h) \quad \forall v_h \in X_h \\ b(u_h, \mu_h) = 0 \quad \forall \mu_h \in M_h. \end{array} \right. \quad (14)$$

Spaces  $X_h$  and  $M_h$  can be taken “independent” from each other. For instance,  $X_h$  can be a P1 or Q1 finite elements space based on a regular mesh in  $C$  and  $M_h$  is some finite element space constructed from the discretization of  $\gamma$  (see Fig. 4).  $X_h$  and  $M_h$  will be assumed to satisfy the usual approximation properties

$$\begin{cases} \lim_{h \rightarrow 0} \inf_{(v_h \in X_h)} \|u - v_h\|_X = 0 & \forall u \in X \\ \lim_{h \rightarrow 0} \inf_{(\mu_h \in M_h)} \|\mu - \mu_h\|_M = 0 & \forall \mu \in M. \end{cases} \quad (15)$$

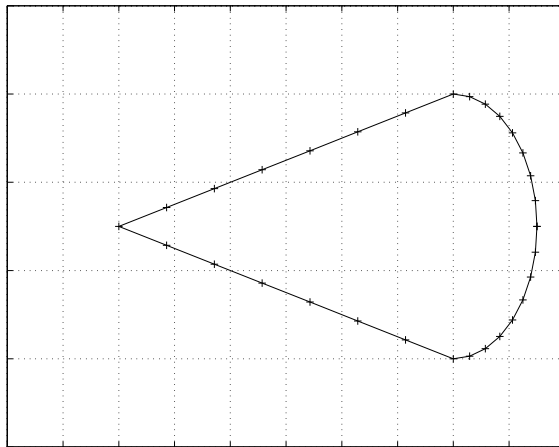


Fig 4: *Example of the two meshes in 2D*

Here, remembering that  $M_h$  is a subspace of  $H^{-1/2}(\gamma)$ , it makes sense to use discontinuous functions to construct  $X_h$  and then use, for instance, piecewise constant functions.

Let us introduce  $\{v_j, 1 \leq j \leq p = \dim X_h\}$  and  $\{w_\ell, 1 \leq \ell \leq q = \dim M_h\}$  two bases for the spaces  $X_h$  and  $M_h$ . We have  $p = O(1/h^d)$  and  $q = O(1/h^{d-1})$ , so  $q$  is generally much less than  $p$ .

Let us define

- $M_h$  = the  $p \times p$  mass matrix associated with the scalar product  $(u_h, v_h)$
- $A_h$  = the  $p \times p$  stiffness matrix associated with the bilinear form  $a(u_h, v_h)$

- $B_h =$  the  $q \times p$  "boundary" matrix associated with the bilinear form  $b(u_h, \mu_h)$

If  $U_h$  (respectively  $\Lambda_h$ ) is the column vector representing the decomposition of  $u_h$  (respectively  $\lambda_h$ ) on the base  $\{v_j\}$  (respectively  $\{w_\ell\}$ ), we have

$$\begin{cases} M_h \frac{d^2 U_h}{dt^2} + A_h U_h = B_h^t \Lambda_h \\ B_h U_h = 0, \end{cases} \quad (16)$$

where  $B_h^t$  is the transpose of  $B_h$ . If  $M_h$  and  $A_h$  can be interpreted respectively as approximations of the identity and Laplace operators,  $B_h$  can be seen as a discrete trace operator from  $X_h$  to  $M_h$ . Problem (16) appears as a system of ordinary differential equations with an algebraic constraint. This establishes an analogy with problems of fluid dynamics in the incompressible case where the free divergence is the constraint.

**Remark :** In the following, the elements of the mass matrix  $M_h$  are supposed to be calculated via an appropriate quadrature formula in such a way that  $M_h$  becomes diagonal (mass lumping). For lower order Lagrange elements, such a procedure is well known. The case of higher order elements can be handled using the ideas developed in [6]. Mass lumping allows us to get an explicit scheme as we will see below. In the following, we suppose that  $M_h$  is a lumped matrix.

### 2.2.2 Time discretization

For time discretization, the interval of time  $[0, T]$  is divided into  $N$  pieces of length  $\Delta t = \frac{T}{N}$ . Time step  $\Delta t$  must be chosen in accordance with the space step of the mesh defined on the computational domain in order to satisfy the stability conditions, as will be seen later. We

use the three time step finite difference explicit scheme for the time derivatives

$$\begin{cases} U_h^{n+1} - 2U_h^n + U_h^{n-1} = -\Delta t^2 M_h^{-1} A_h U_h^n + \Delta t^2 M_h^{-1} B_h^t \Lambda_h^n & (1) \\ B_h U_h^n = 0. & (2) \end{cases} \quad (17)$$

To compute the solution explicitly, an apparent difficulty appears with the condition  $B_h U_h^n = 0$ . In fact for practical computation, the condition ((17)-(2)) is replaced by an equivalent condition which results from multiplying the first equation by  $B_h$ :

$$B_h(U_h^{n+1} - 2U_h^n + U_h^{n-1}) = -\Delta t^2 B_h M_h^{-1} A_h U_h^n + \Delta t^2 B_h M_h^{-1} B_h^t \Lambda_h^n. \quad (18)$$

Because equation ((17)-(2)) holds at each time step, the left side of equation (18) vanishes.

Finally, we obtain the system

$$\begin{cases} U_h^{n+1} = 2U_h^n - U_h^{n-1} - (\Delta t)^2 M_h^{-1} A_h U_h^n + (\Delta t)^2 M_h^{-1} B_h^t \Lambda_h^n & (1) \\ B_h M_h^{-1} B_h^t \Lambda_h^n = B_h^t M_h^{-1} A_h U_h^n. & (2) \end{cases} \quad (19)$$

Similarly, multiplying the first equation of system (19) by  $B_h^t$  and using equation (2) of system (19) leads to

$$\begin{cases} U_h^{n+1} = 2U_h^n - U_h^{n-1} - \Delta t^2 M_h^{-1} A_h U_h^n + (\Delta t)^2 M_h^{-1} B_h^t \Lambda_h^n \\ B_h(U_h^{n+1} - 2U_h^n + U_h^{n-1}) = 0. \end{cases} \quad (20)$$

If we suppose that at initial times ( $n = 0, n = 1$ ) the condition  $B_h U_h^n = 0$  holds, by induction over  $n$ , it is easy to see that the condition  $B_h U_h^n = 0$  is true for all time. So system (19) implies system (17).

In conclusion, systems (17) and (19) are equivalent as soon as we have at initial times

$$B_h U_h^0 = B_h U_h^1 = 0, \quad (21)$$

which is in fact nothing but a compatibility condition between the boundary and initial conditions.

Finally, let us assume  $(U_h^{n-1}, U_h^n)$  to be known; then  $(U_h^n, U_h^{n+1})$  is computed by the following procedure:

- first, solve equation  $B_h M_h^{-1} B_h^t \Lambda_h^n = B_h M_h^{-1} A_h U_h^n$  to get the Lagrange multiplier  $\Lambda_h^n$ ,
- second, get the wave solution at  $n + 1$  via ((19)-(1)).

For the computation of the Lagrange multiplier, we must invert the matrix  $Q = B_h M_h^{-1} B_h^t$ .

In the following, we make some remarks about the matrix  $Q$ .

### 2.3 Properties of the matrix $Q$

The following properties of the matrix  $Q = B_h M_h^{-1} B_h^t$  are easily derived:

- $Q$  is symmetric and positive
- The size of  $Q$  is exactly  $(q, q)$  which is very small compared to the size of matrix  $A_h$  since in practice we have  $q \ll p$ .
- $Q$  is a sparse matrix with narrow bandwidth (see section 4.2).

The last property is linked to the sparsity of the matrix  $B_h$ . This matrix couples the solution  $u_h$  to the Lagrange multiplier  $\lambda_h$  and its coefficient  $b(v_i, w_j)$  vanishes if the support of the two basis functions  $(v_i, w_j)$  do not intersect.

Thus, if  $Q^{-1}$  exists, then the inversion of  $Q$  can be performed by a Cholesky factorization or by a conjugate gradient algorithm. There remains the crucial question of the existence

of this inverse. Definiteness of  $Q$  is ensured as soon as the kernel of the matrix  $B_h^t$  is equal to 0. This is related to a property of the continuous variational problem. More precisely, the key condition for the existence of the multiplier  $\lambda$  in the variational formulation (5) is the inf-sup condition,

$$\inf_{(\lambda \in \mathbf{M})} \sup_{(v \in \mathbf{X})} \frac{b(v, \lambda)}{\|\lambda\|_{\mathbf{M}} \|v\|_{\mathbf{X}}} = C > 0. \quad (22)$$

Similarly, the existence of  $(u_h, \lambda_h)$  and the convergence of the method when  $h$  tends to zero is linked to the uniform discrete inf-sup condition,

$$\exists C', \text{ independent of } h \text{ such that } \inf_{(\lambda \in \mathbf{M}_h)} \sup_{(v \in \mathbf{X}_h)} \frac{b(v, \lambda)}{\|\lambda\|_{\mathbf{M}} \|v\|_{\mathbf{X}}} = C' > 0. \quad (23)$$

This condition requires a compatibility relation between the two meshes. It imposes a condition between the dimensions of the two spaces  $\mathbf{X}_h$  and  $\mathbf{M}_h$ . Such a condition can be found in [13] where elliptic problems are studied. More precisely, it is demonstrated theoretically that if the space increment  $h_s$  used for the discretization of the obstacle is three times larger than the space increment  $h_v$  used for the regular squared mesh, the uniform inf-sup condition holds. However numerical experiments show that this condition can be relaxed from three to a number slightly larger than one. In any case,  $h_v$  must be smaller than  $h_s$ . Consequently, for a given space increment, it is impossible to use the FDM for obstacles whose geometry is very irregular with respect to  $h_v$ .

## 2.4 About error estimates

Here, we estimate the error between the approximate solution  $(u_h, \lambda_h)$  of the semi-discrete problem (14) and the exact solution  $(u, \lambda)$  of problem (5) provided that this solution is regular enough. To do so, we suppose that the uniform discrete condition (23) is fulfilled. Following Dupont [9] or Brezzi [5], we introduce the elliptic operator defined from  $\mathbf{X} \times \mathbf{M}$

to  $\mathbf{X}_h \times \mathbf{M}_h$  by

$$\Pi_h(u, \lambda) = (\Pi_h u, \Pi_h \lambda), \quad \text{and} \quad (24)$$

$$\begin{cases} a(u - \Pi_h u, v_h) = b(v_h, \lambda - \Pi_h \lambda) & \forall v_h \in \mathbf{X}_h \\ b(u - \Pi_h u, \mu_h) = 0 & \forall \mu_h \in \mathbf{M}_h. \end{cases} \quad (25)$$

It can be shown [5] that the uniform inf-sup condition joined to the coercivity of the bilinear form  $a$  ensures the existence and the uniqueness of  $\Pi_h$ .

Using  $\Pi_h$ , the error between the approximate solution and the exact solution is split into two parts

$$\begin{cases} u - u_h(t) = (u(t) - \Pi_h u(t)) + (\Pi_h u(t) - u_h(t)) = \epsilon_h(t) + \eta_h(t) \\ \lambda - \lambda_h(t) = (\lambda(t) - \Pi_h \lambda(t)) + (\Pi_h \lambda(t) - \lambda_h(t)) = \theta_h(t) + \tau_h(t). \end{cases} \quad (26)$$

By setting

$$\|(u, \lambda) - \Pi_h(u, \lambda)\| = \|u(t) - \Pi_h u(t)\|_{\mathbf{X}} + \|\lambda(t) - \Pi_h \lambda(t)\|_{\mathbf{M}}, \quad (27)$$

we have the classical result

$$\begin{cases} \exists \sigma, \text{ independent of } h \text{ such that} \\ \|(u, \lambda) - \Pi_h(u, \lambda)\| \leq \sigma \left\{ \inf_{v_h \in \mathbf{X}_h} \|u(t) - v_h\|_{\mathbf{X}} + \inf_{\mu_h \in \mathbf{M}_h} \|\lambda(t) - \mu_h\|_{\mathbf{M}} \right\}. \end{cases} \quad (28)$$

This shows, by (15), that  $\epsilon_h$  and  $\theta_h$  tend to zero uniformly in time ( $t \in [0, T]$ ). In the same way, if  $(u, \lambda) \in \mathcal{C}^3(0, T; \mathbf{X}) \times \mathcal{C}^3(0, T; \mathbf{M})$  the same estimates hold for the second and third

time derivatives of the errors. In particular

$$\left\{ \begin{array}{l} \exists \sigma, \text{ independent of } h \text{ such that if } k = 2, 3, \forall t \geq 0 \\ \left\| \frac{d^k \epsilon_h}{dt^k} \right\|_{\mathbf{X}} \leq \sigma \left\{ \inf_{(v_h \in \mathbf{X}_h)} \left\| \frac{d^k u(t)}{dt^k} - v_h \right\|_{\mathbf{X}} + \inf_{(\mu_h \in \mathbf{M}_h)} \left\| \frac{d^k \lambda(t)}{dt^k} - \mu_h \right\|_{\mathbf{M}} \right\}. \end{array} \right. \quad (29)$$

Let us assume that

$$\left\{ \begin{array}{l} u_h(0) = \Pi_h u(0) \\ \frac{du_h}{dt}(0) = \Pi_h \frac{du}{dt}(0) \end{array} \right. \quad (30)$$

(i.e, we impose no error at time  $t = 0$  to simplify), then with appropriate energy estimates,

we obtain (see Appendix 1)

$$\left\{ \begin{array}{l} \|\eta_h(t)\|_{\mathbf{X}} \leq \left(\frac{t^2}{2} + t\right) \sup_{[0,t]} \left| \frac{d^2 \epsilon_h}{dt^2} \right| \\ \|\tau_h(t)\|_{\mathbf{M}} \leq \frac{1}{C'} \left( M \left(\frac{t^2}{2} + t\right) + 1 \right) \sup_{s \in [0,t]} \left| \frac{d^2 \epsilon_h}{dt^2} \right| + t \sup_{s \in [0,t]} \left| \frac{d^3 \epsilon_h}{dt^3} \right|. \end{array} \right. \quad (31)$$

In equation (31), we have denoted by  $M$  the continuity constant of the bilinear form  $a(.,.)$

$$a(u, v) \leq M \|u\|_{\mathbf{X}} \|v\|_{\mathbf{X}} \quad \forall (u, v) \in \mathbf{X} \times \mathbf{X}, \quad (32)$$

and by  $C'$  the constant for the inf-sup condition. In conclusion, all the quantities  $(\epsilon_h(t), \theta_h(t), \eta_h(t), \tau_h(t))$  go to zero when  $h$  vanishes, uniformly for  $t$  in any bounded interval, as soon as the uniform discrete inf-sup condition is met. This implies that the error between the exact solution of problem (5) and the approximate solution of the semi-discrete problem (14) converges to zero as  $h$  tends to zero.

## 2.5 Stability

In this section, the stability of the numerical scheme is studied. The remarkable result is that our new scheme is stable under exactly the same conditions as in the case without an obstacle. We define the discrete energy

$$E_h^{n+1/2} = \frac{1}{2} \left\{ \left| \frac{u_h^{n+1} - u_h^n}{\Delta t} \right|^2 + a(u_h^{n+1}, u_h^n) \right\}. \quad (33)$$

We remark that scheme (17) is the “matrix form” of the following variational scheme

$$\begin{cases} \left( \frac{u_h^{n+1} - 2u_h^n + u_h^{n-1}}{\Delta t^2}, v_h \right) + a(u_h^n, v_h) = b(v_h, \lambda_h^n) & \forall v_h \in X_h \\ b(u_h^n, \mu_h) = 0 & \forall \mu_h \in M_h. \end{cases} \quad (34)$$

Taking  $v_h = \frac{u_h^{n+1} - u_h^{n-1}}{2\Delta t}$ , we obtain

$$\frac{E_h^{n+1/2} - E_h^{n-1/2}}{\Delta t} + b\left(\frac{u_h^{n+1} - u_h^{n-1}}{2\Delta t}, \lambda_h^n\right) = 0. \quad (35)$$

Then if we take  $\mu_h = \lambda_h^{n-1}$  (respectively  $\mu_h = \lambda_h^{n+1}$ ), we see that  $b(u_h^n, \lambda_h^{n-1}) = 0$  (respectively  $b(u_h^n, \lambda_h^{n+1}) = 0$ ) for all  $n$ . Therefore  $b\left(\frac{u_h^{n+1} - u_h^{n-1}}{2\Delta t}, \lambda_h^n\right) = 0$ . So the discrete energy  $E_h^{n+1/2}$  is conserved.

Rewriting (33) as

$$\begin{aligned} E_h^{n+1/2} &= \frac{1}{2} \left| \frac{u_h^{n+1} - u_h^n}{\Delta t} \right|^2 \\ &\quad - \frac{1}{2} a\left(\frac{u_h^{n+1} - u_h^n}{2}, \frac{u_h^{n+1} - u_h^n}{2}\right) + \frac{1}{2} a\left(\frac{u_h^{n+1} + u_h^n}{2}, \frac{u_h^{n+1} + u_h^n}{2}\right), \end{aligned} \quad (36)$$

the discrete energy  $E_h^{n+1/2}$  is a positive quadratic form in  $(u_h^n, u_h^{n+1})$  as soon as

$$|v_h|^2 - \frac{(\Delta t)^2}{4} a(v_h, v_h) > 0 \quad \forall v_h \in X_h. \quad (37)$$

In this case, there is conservation of discrete energy and the scheme is  $L^2$  stable. Condition (37) is nothing else than the usual CFL condition

$$\frac{\Delta t}{h} < \alpha_{CFL}, \quad (38)$$

where  $\alpha_{CFL}$  is the stability threshold defined by

$$\alpha_{CFL}^2 = \left\{ \sup_{u \in X_h} \frac{h^2 a(u, u)}{4 |u|^2} \right\}^{-1}. \quad (39)$$

### 3 Fictitious domain solution for the Maxwell equations

#### 3.1 Generalities

We deal with the scattering of an electromagnetic wave by a perfect conductor denoted by  $\mathcal{O}$  ( $\mathcal{O} \subset \mathbf{R}^d$  with  $d = 2$  or  $d = 3$ ). We reuse the same abstract formalism as in Section 2. Let us first rewrite the Maxwell equations in term of the only electric field. The field satisfies the equations

$$\begin{cases} \frac{\partial^2 \vec{E}}{\partial t^2} + \text{curl}(\text{curl} \vec{E}) = 0 & \text{in } \mathbf{R}^d \setminus \mathcal{O} \\ \vec{n} \wedge (\vec{E} \wedge \vec{n}) = 0 & \text{on } \gamma. \end{cases} \quad (40)$$

A Dirichlet condition or an absorbing boundary condition is assumed on the exterior boundary of the rectangular computation domain. This problem can still be written in

the abstract form (5) with the following identifications:

$$\left\{ \begin{array}{l} u = \vec{E} \text{ is the electric field} \\ v = \vec{F} \text{ is the associated test function} \\ X = \mathbb{H}(\text{curl}, C) \\ M = \mathbb{H}^{-1/2}(\text{div}_\gamma, \gamma) \text{ if } d = 3 \text{ and } M = \mathbb{H}_t^{1/2}(\gamma) \text{ if } d = 2 \\ (u, v) = \int_C uv \, dx \\ a(u, v) = \int_C \text{curl}(u)\text{curl}(v) \, dx \\ b(u, \lambda) = \int_\gamma \vec{n} \wedge (\vec{E} \wedge \vec{n}) \cdot \lambda \, d\gamma. \end{array} \right. \quad (41)$$

Let us recall that  $\mathbb{H}^{-1/2}(\text{div}_\gamma, \gamma) = \{v/v \in \mathbb{H}_t^{-1/2}(\gamma), \text{div}_\gamma(v) \in \mathbb{H}_t^{-1/2}(\gamma)\}$  and

$\mathbb{H}_t^{-1/2} = \{v/v \in \mathbb{H}^{-1/2}(\gamma) / \langle v, \phi \rangle = 0 \, \forall \phi \in \mathbb{H}^{1/2}(\gamma) / \phi \wedge n = 0\}$  (see ([8],[16]) for more details) and  $\text{div}_\gamma(v)$  is the tangential divergence on  $\gamma$ .

Physically, it is interesting to notice that the Lagrange multiplier represents the derivative in time of a surface current localized on the perfect conductor. In the following, we shall discuss the finite element approximation of problem (40)-(41).

## 3.2 Finite element approximation

### 3.2.1 Elements of $\mathbf{X}_h$ :

In order to take advantage of the FDM, we use regular grids for discretizing the domain  $C$ . In the 2D (respectively 3D) case, we use squares (respectively cubes). We consider for simplicity the lowest order Nédelec elements of the space  $\mathbb{H}(\text{curl})$ [19]. The degrees of freedom of such elements are the values of the tangential component at the middle of the

edges. A corresponding set of basis functions is obtained by associating to each edge the function whose tangential component is equal to one on that edge and equal to zero on the others.

The electric field is equal to  $\vec{E} = \sum_{k=1}^p E_k \vec{v}_k$ , where  $p$  is the number of degrees of freedom in the space  $H(\text{curl})$ .

### 3.2.2 Elements of $M_h$ :

In the 2D case, the Lagrange multiplier belongs to  $H_t^{1/2}(\gamma)$ . We can approximate the boundary  $\gamma$  by segments and choose the P1 elements for the approximation of the Lagrange multiplier. In the 3D case, the Lagrange multiplier belongs to  $H^{-1/2}(\text{div}_\gamma, \gamma)$ . The boundary which is now a surface, can be approximated by triangles and we can choose the lowest order Raviart-Thomas elements for  $M_h$  ([12], [20]). The degrees of freedom are the values of the normal components at the middle of the edges.

The multiplier can be written  $\vec{\lambda} = \sum_{k=1}^q \Lambda_k \vec{w}_k$  where  $q$  is the number of degrees of freedom.

### 3.2.3 The discrete variational problem:

The problem is rewritten in the abstract form (16). The matrices are now defined by  $M_h(l, k) = \int_C \vec{v}_l \vec{v}_k dx$  for the mass matrix,  $A_h(l, k) = \int_C \text{curl}(\vec{v}_l) \text{curl}(\vec{v}_k) dx$  for the stiffness matrix and  $B_h(k, l) = \int_\gamma \vec{v}_l \vec{w}_k dx$  for the “boundary matrix ”.

### 3.2.4 Time discretization

We have used the standard finite difference scheme for the time derivatives. After mass lumping, the problem to be solved is

$$\begin{cases} E_h^{n+1} - 2E_h^n + E_h^{n-1} = -\Delta t^2 M_h^{-1} A_h E_h^n + \Delta t^2 M_h^{-1} B_h^t \Lambda_h^n & (1) \\ B_h E_h^n = 0. & (2) \end{cases} \quad (42)$$

On a regular mesh, the electric field at time  $n\Delta t$  can be split in two parts

$$\vec{E}(n\Delta t) = \sum_{i,j} E_{i+\frac{1}{2},j}^n \vec{x} + \sum_{i,j} E_{i,j+\frac{1}{2}}^n \vec{y}, \quad (43)$$

where  $E_{i+\frac{1}{2},j}^n$  denotes the  $x$ -component of the electric field at time  $n \times \Delta t$  and at point  $((i + \frac{1}{2}) l_x, j l_y)$  (i.e at a point located at the middle of a horizontal wedge) and  $E_{i,j+\frac{1}{2}}^n$  is defined similarly. Without the obstacle, the scheme is written as

$$\left\{ \begin{array}{l} E_{i+\frac{1}{2},j}^{n+1} = 2E_{i+\frac{1}{2},j}^n - E_{i+\frac{1}{2},j}^{n-1} \\ \quad + \frac{\Delta t^2}{l_y^2} (-E_{i+\frac{1}{2},j+1}^n + 2E_{i+\frac{1}{2},j}^n - E_{i+\frac{1}{2},j-1}^n) \\ \quad + \frac{\Delta t^2}{l_x l_y} (E_{i,j-\frac{1}{2}}^n - E_{i+1,j-\frac{1}{2}}^n - E_{i+1,j+\frac{1}{2}}^n - E_{i,j+\frac{1}{2}}^n) \quad i = 1, \dots, p \\ \\ E_{i,j+\frac{1}{2}}^{n+1} = 2E_{i,j+\frac{1}{2}}^n - E_{i,j+\frac{1}{2}}^{n-1} \\ \quad + \frac{\Delta t^2}{l_x^2} (-E_{i+1,j+\frac{1}{2}}^n + 2E_{i,j+\frac{1}{2}}^n - E_{i-1,j+\frac{1}{2}}^n) \\ \quad + \frac{\Delta t^2}{l_x l_y} (E_{i-\frac{1}{2},j}^n - E_{i-\frac{1}{2},j+1}^n - E_{i+\frac{1}{2},j+1}^n - E_{i+\frac{1}{2},j}^n) \quad j = 1, \dots, q. \end{array} \right. \quad (44)$$

One of the important properties of this scheme is that it can be reinterpreted in the framework of the finite-difference time-domain method or FDTD, [21]. Let us consider the system

$$\left\{ \begin{array}{l} \frac{H^{n+1/2} - H^{n-1/2}}{\Delta t} + R_h E^n = 0 \\ \frac{E^{n+1} - E^n}{\Delta t} - R_h^t H^{n+1/2} = \frac{1}{h^2} B_h^t \lambda^{n+1/2} \\ B_h E^n = 0, \end{array} \right. \quad (45)$$

where  $R_h$  stands for the discrete curl operator constructed on staggered grids of steps  $h$  and  $R_h^t$  for its transpose. If we forget about the term in  $\lambda^{n+1/2}$ , the two first equations

in (45) are nothing else than the classical Yee scheme for the FDTD, [22]. From (45), we

deduce

$$\left\{ \begin{array}{l} \frac{1}{\Delta t} \left( \frac{E^{n+1} - E^n}{\Delta t} - \frac{E^n - E^{n-1}}{\Delta t} \right) - R_h^t \left( \frac{H^{n+1/2} - H^{n-1/2}}{\Delta t} \right) \\ = \frac{1}{h^2} B_h^t \left( \frac{\lambda^{n+1/2} - \lambda^{n-1/2}}{\Delta t} \right), \end{array} \right.$$

or

$$h^2 \frac{E^{n+1} - 2E^n + E^{n-1}}{\Delta t^2} + h^2 R_h^t R_h E^n = B_h^t \Lambda_h^n,$$

where we have set

$$\frac{\lambda^{n+1/2} - \lambda^{n-1/2}}{\Delta t} = \Lambda^n.$$

If we remark that the assembly of the mass matrix and stiffness matrices for the lowest order Nédelec's elements calculated with mass lumping [18] and for isotropic meshes (i.e.  $l_x = l_y = h$ ) gives

$$M_h = h^2 Id, \quad A_h = h^2 R_h^t R_h,$$

we finally obtain equivalence between systems (42) and (45).

As suggested in [7], the scheme can be solved into

$$\left\{ \begin{array}{l} H^{n+1/2} = H^{n-1/2} - \Delta t R_h E^n \\ E_{FDTD}^{n+1} = E^n + \Delta t R_h^t H^{n+1/2} \\ \Lambda^n = \left( B_h \frac{1}{h^2} B_h^t \right)^{-1} B_h E_{FDTD}^{n+1} \\ E^{n+1} = E_{FDTD}^{n+1} - \frac{\Delta t}{h^2} B_h^t \Lambda^n. \end{array} \right. \quad (46)$$

In system (46), the obstacle is incorporated inside the scheme by modifying the classical two-step FDTD. At first, the surface current  $\Lambda^n$  is determined by solving the small linear system with matrix  $B_h B_h^t$ ; then, the electric field is modified to take into account this

current. What we finally propose here is to include diffraction effects by simply adding two steps to the classical calculation. This remark is important as most of the usual codes for transient electromagnetics are based on FDTD.

In the next part, numerical results are presented with a Dirichlet condition on the outer boundary of the obstacle or with a second order absorbing boundary condition. Note that the choice of the conditions at the boundary is crucial to bound the computation domain but is not related with the implementation of the FDM.

## 4 Numerical experiments

### 4.1 Generalities

The FDTD has been used extensively to compute scattering from perfectly conducting targets, [21]. We propose to adapt the FDM to improve the computation of electromagnetic scattering for obstacles of complicated shapes in this context (as seen in Section 3.2.5, the final numerical scheme is only a slight perturbation of the FDTD equations). Our aim is to demonstrate that the solution obtained from the FDM is better in terms of accuracy than the solution obtained by approximating the exact boundary by a staircase discrete boundary. In fact, simple problems in 2D are presented.

The test problems to be discussed concern the solution of the problem described in Section 3.1, 3.2. We perform a Cholesky factorization of the matrix  $B_h M_h^{-1} B_h^t$  before starting the time iterations.

### 4.2 Computation of the matrix $B$

The matrix  $B_h$  can be seen as a discrete trace operator from  $X_h$  to  $M_h$  and can be written as a line integral

$$B_h(i, j) = \int_{\gamma} \vec{v}_j \vec{w}_i ds. \quad (47)$$

For more simplicity, we have chosen to take the  $P^0$  element basis for the discretization of the space  $M$ . In theory, this choice does not fit the general framework described in Sections 2 and 3 since piecewise constant functions do not belong to  $H^{1/2}$ . However, since we choose a subspace of  $L^2$  for approximating both  $H^{1/2}$  and  $H^{-1/2}$ , the bilinear form  $b(v, \lambda)$  defined by (47) still makes sense as an integral in the discrete case, which justifies our choice.

The computation of the integral (47) can be done in two ways. First it is evaluated by means of an exact computation requiring the intersection between the volume and surface meshes  $X_h$  and  $M_h$  and some integration of quadratic functions. Second, the integral can be done with an approximate computation based on a Riemann sum.

The numerical implementation of the Riemann method is very easy and can be used to test the first method. But the method based on the exact computation appears to be more efficient in computation time.

We show in Fig. 5 the sparsity pattern of the matrix  $Q = B_h M_h^{-1} B_h^t$  when the obstacle is a disk and when  $h_s$  is equal to  $h_v$ . Let us recall that  $h_v$  (respectively  $h_s$ ) is the space increment used for the discretization of the computational domain (respectively of the boundary). The matrix  $Q$  has 2 % nonzero coefficients and its bandwidth is equal to 8. In figure 6, is depicted the condition number of the matrix versus  $h_s/h_v$  for two types of geometries. As a result, the condition number of the matrix is better as  $h_s/h_v$  increases and this independently of the shape of the obstacle.

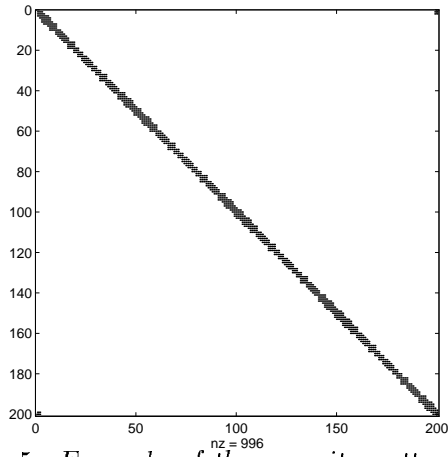


Fig 5: *Example of the sparsity pattern of the matrix  $Q$  where  $nz$  is the number of nonzero coefficients*

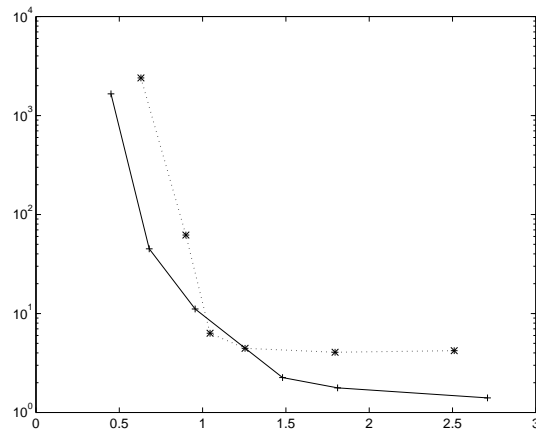


Fig 6: *Matrix condition number versus  $h_s/h_v$  ( - :when the obstacle is a inclined plane and ...: when the obstacle is a disk)*

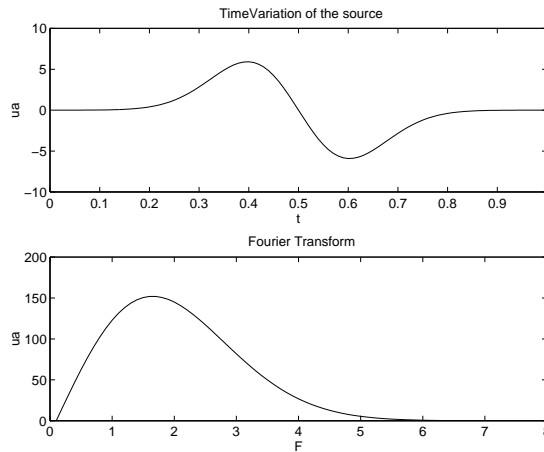


Fig 7: *Time evolution of the source and its Fourier transform*

### 4.3 A first test: reflection on a plane

A first experiment deals with the reflection on a plane of a wave produced by a point source in 2D

$$S(p, t) = g(t) \operatorname{curl}(\delta(p - p_s) \cdot \vec{e}_3), \quad g(t) = \frac{d}{dt} \left( \exp^{-(t/t^0)^2} \right), \quad (48)$$

where  $\vec{e}_3$  is the vector perpendicular to the computational plane.  $t^0$  is equal to 0.145 s and  $p_s$  is a point located at 0.68 m from the reflecting plane (see Fig. 7). We consider two cases: the reference case where the plane is vertical (noted case A) and the test case where the plane is inclined at an angle  $\theta$  with the vertical plane (noted case B). In case A, the object is discretized on the regular grid mesh. The finite difference method and the FDM give the same results. On the contrary, in case B, the object does not coincide with the regular grids. Figures 8-9 compare two snapshots taken at the same instant and computed by the FDM for the two positions of the reflecting plane. We have drawn the level curves of the tangential component of the electric field at time  $t = 1.26s$ . On the right side of the figure, the propagation of the point source can be seen. The reflection of the conducting plane appears on the left side of the figures. We can see the distortion of the wave surface. Because we have extended the fields to all the computational domain, small values of the tangential field are located on the left of the position of the conducting plane. A good

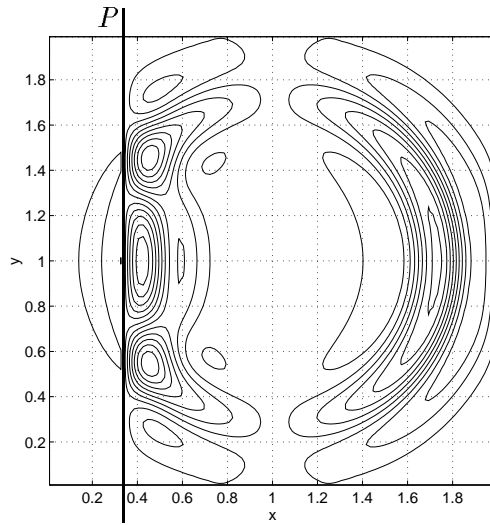


Fig 8: Snapshot at  $t = 1.26$  s. of the tangential component of the electric field with a vertical reflecting plane  $P$

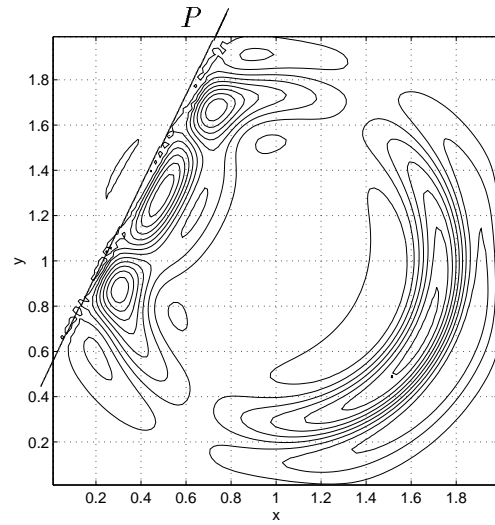


Fig 9: Snapshot at  $t = 1.26$  s. of the tangential component of the electric field when the plane  $P$  is inclined at an angle of 28 degrees

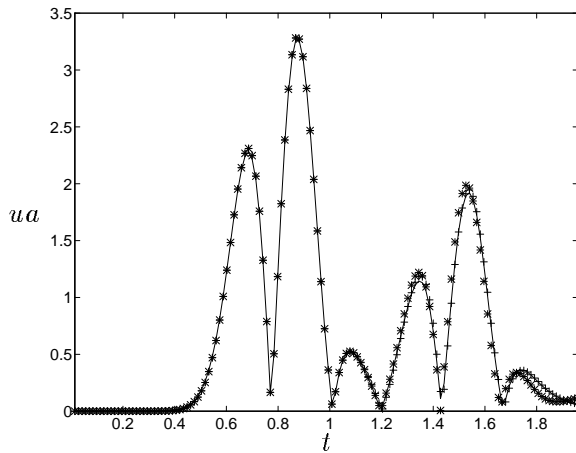


Fig 10: Trace-recording of the modulus of the electric field ( $ua$ ) versus time ( $t$ ) ( - :reference case, +: test case, \*: stair case) ( $h_v=h_s=0.02$ )

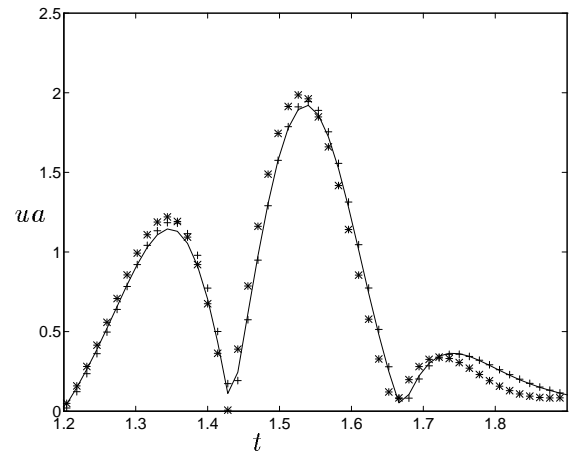


Fig 11: Zoom of Figure 10

agreement of the two pictures (8-9) can be seen.

We compare now the FDM with the solution obtained the method using the staircase approximation of the boundary. Figures 10-14 give the trace-recording of the modulus of the electric field at a point  $p_M$  located at  $0.34m$  from the reflecting plane. From the initial time to the time  $t = 1.2s$ , we see only the propagation of the point source. After the time  $t = 1.2s$ , reflected waves are present. Figure 11 (zoom of Figure 10) is more interesting

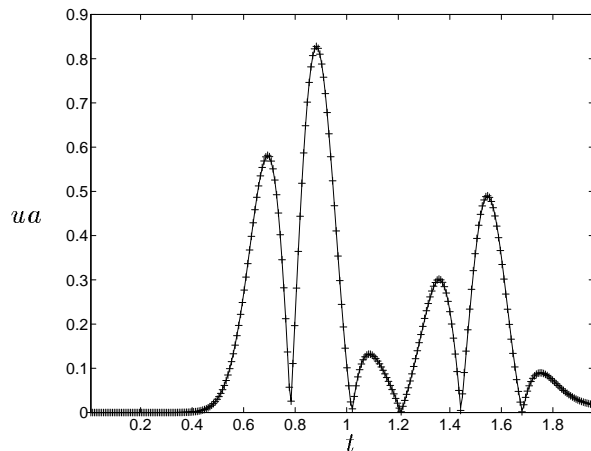


Fig 12: Same as Figure 10 but with  $h_v = h_s = 0.01$

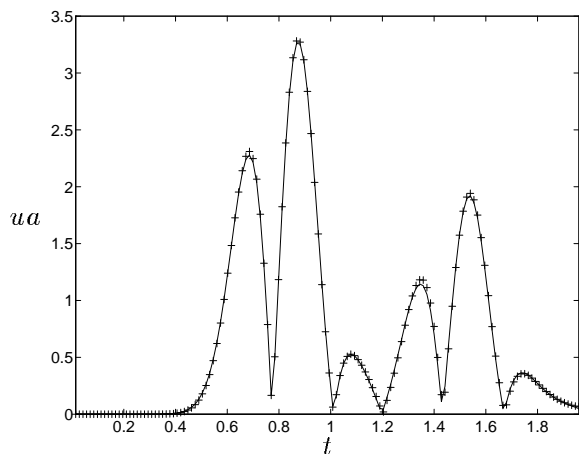


Fig 13: Same as Figure 10 but with  $h_v = 0.02$ ,  $h_s = 0.03$

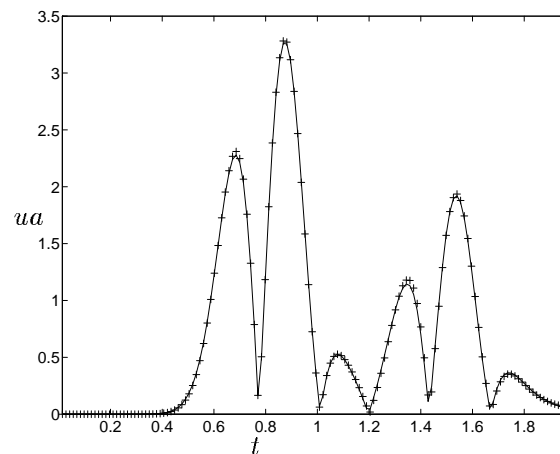


Fig 14: Same as Figure 10 but with  $h_v = 0.02$ ,  $h_s = 0.04$

since it plots the area of time corresponding to the arrival of reflected waves. It clearly shows the gain in accuracy due to the FDM when one discretizes with 10 points per shortest wavelength ( $\lambda^- = 0.2 \Rightarrow h_v = 0.02$ ). To verify the stability of the solution obtained from the FDM, we decrease the space increment  $h_v$ . Of course (see Fig 12 corresponding to the same comparison but with  $h_v = 0.01$ ), when the step size goes to zero, all solutions converge to the true solution. Figures 13-14 shows that the quality of the results is not affected when one increases the step on the boundary for a fixed space increment. This is interesting since the computational cost due to the auxiliary unknown determination is

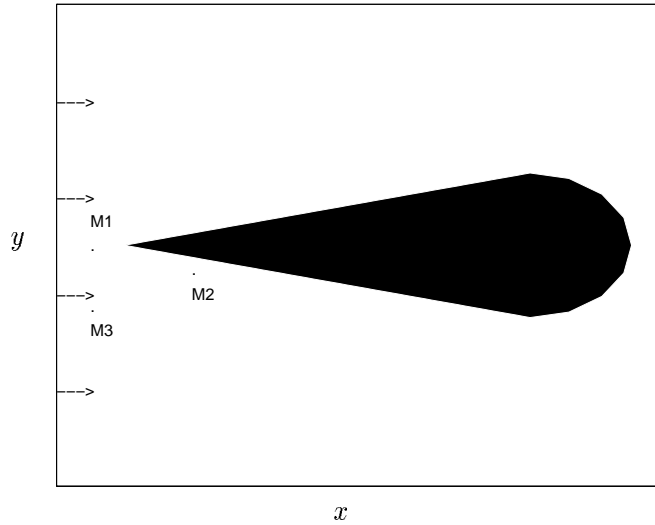


Fig 15: Configuration of the scattering problem in the  $x - y$  plane ( $M1 : (0.3, 1)$ ;  $M2(0.6, 0.9)$ ,  $M3(0.3, 0.75)$ )

linked to the size of the matrix  $Q$  which has been decreased.

#### 4.4 A second test: a wedge

We have computed the electric field reflected by a dihedral (see Fig 15) when it is illuminated by a harmonic wave. The incident electric field propagates in the  $x$ -direction and has only a component on the  $y$ -axis

$$\vec{E}_{inc}(t, x, y) = \frac{dg(t)}{dt} \delta(x - x_s) \vec{e}_y \quad ; g(t) = \left( \exp^{-(t/t^0)^2} \right), \quad (49)$$

where  $x_s$  is an abscissa located at 0.2 from the wedge. Figures 16-17 give the snapshots of the  $y$ -component of the total electric field at different times. On these figures, we can see both the propagation of the incident field and the reflection on the conducting target. First we remark that the wave surface is not planar but is distorted near the obstacle. Secondly, the obstacle also creates a backscattered wave which can be seen in front of the incident field.

Figure 18 shows the trace-recording obtained from the FDM, of the electric field when the

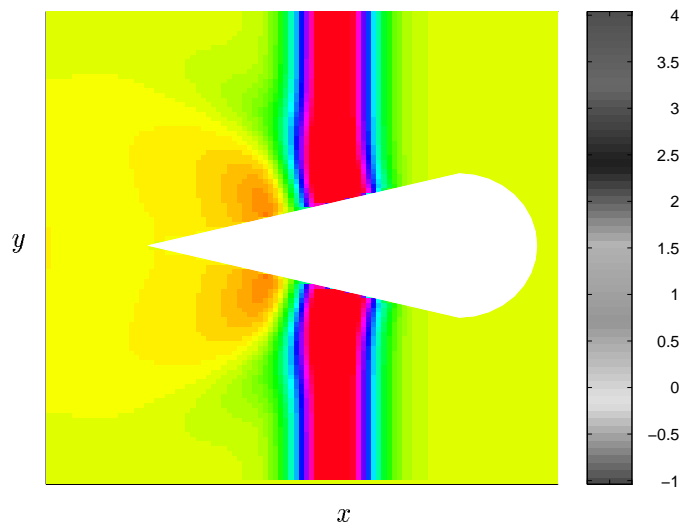


Fig 16: *Snapshot of the  $y$ -component of the electric field at time  $t = 0.13s$*

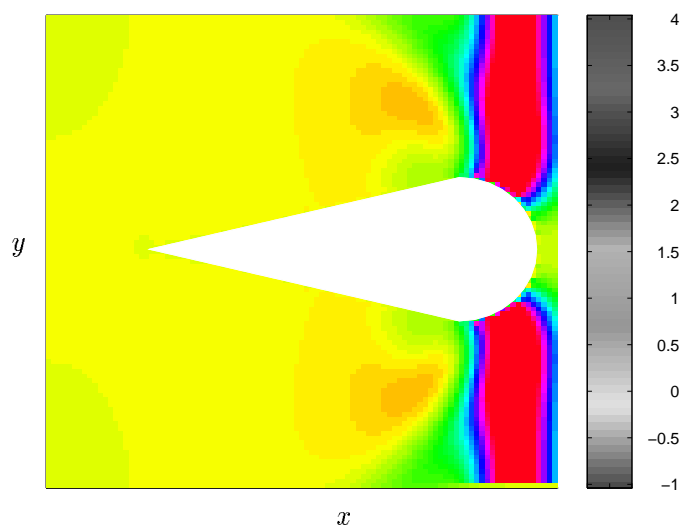


Fig 17: *Same as Fig. 16 but at time  $t = 27s$*

number of points by wavelength is increased. All the curves are close to each other. So a discretization with 10 points per wavelength seems to be adequate for the FDM.

Figures 19-21 compare the amplitude of the electric field obtained with the staircase approximation of the boundary and for various numbers of points per wavelength (10,20,40) with the results obtained by the fictitious method with ten points per wavelength. All the curves obtained with the staircase approximation present oscillations due to the numerical

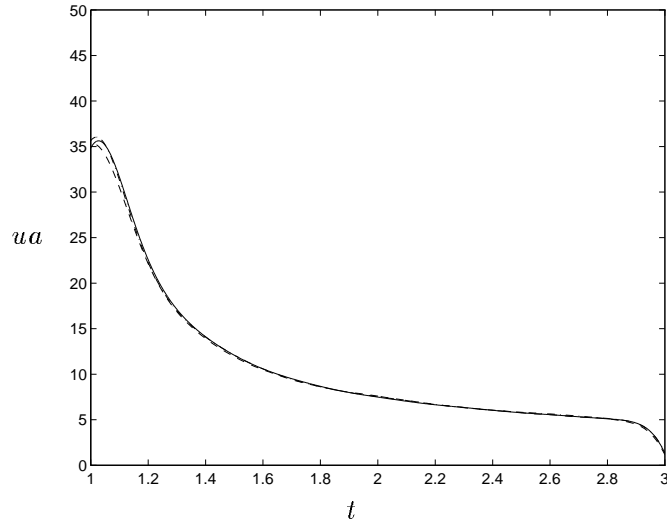


Fig 18: Trace-recording of the modulus of the electric field ( $ua$ ) versus time ( $t$ ) at  $M1$  obtained by the fictitious method for various values of the number of points per wavelength  $nw$  ( $-:nw = 10$ ,  $-. :nw = 20$ ,  $:-nw = 40$ )

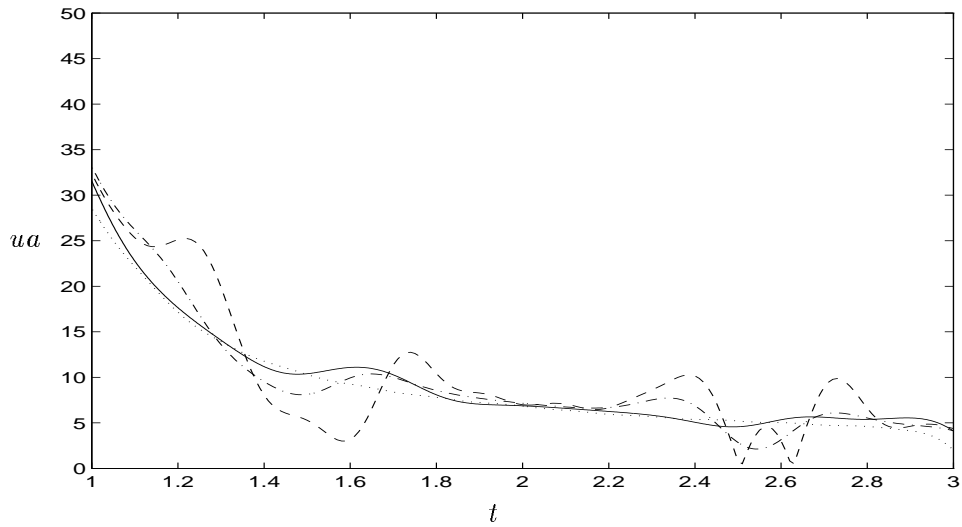


Fig 19: Trace-recording of the modulus of the electric field ( $ua$ ) versus time ( $t$ ) at  $M1$  obtained by ( $\dots$ :fictitious method ( $nw = 10$ ),  $- -$ :FDTD method ( $nw = 10$ ),  $\dots$ :FDTD ( $nw = 20$ ),  $- \cdot$ :FDTD ( $nw = 40$ ))

diffractions. We can also remark that these curves tend to fit the curve obtained from the fictitious domain method when the number of points per wavelength is increased. In conclusion, the fictitious domain method appears to be more efficient in the investigated cases.

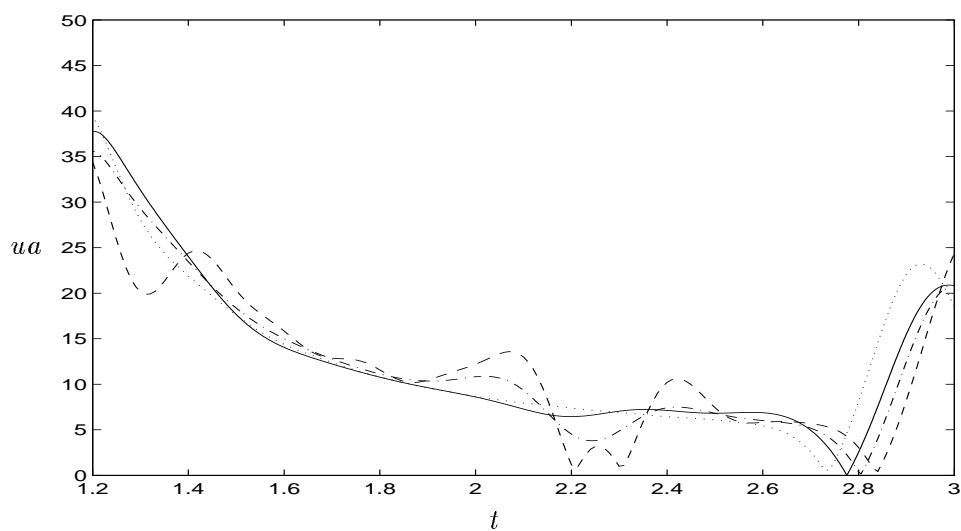


Fig 20: Same as Figure 19 at  $M2 (0.6, 0.9)$

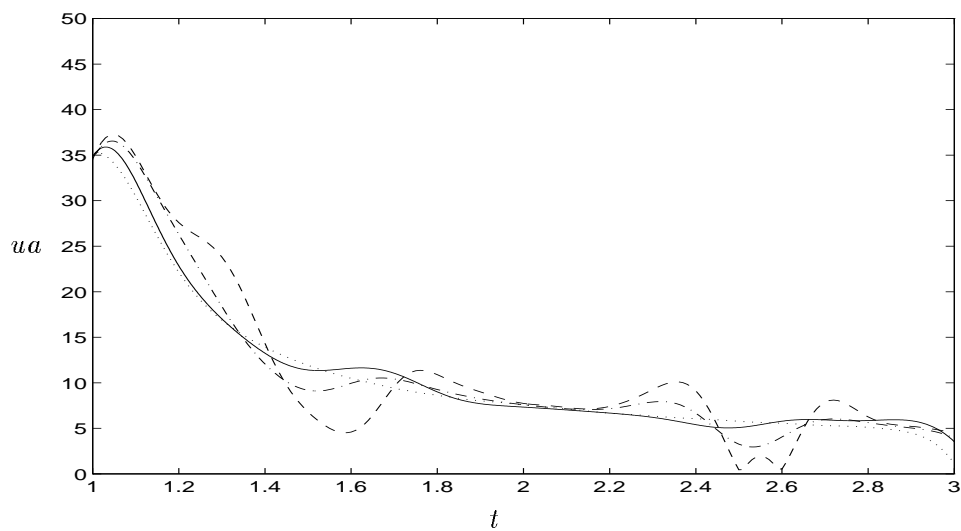


Fig 21: Same as Figure 19 at  $M3 (0.3, 0.75)$

## 5 A plane wave analysis of a 1-D problem

We have shown by numerical examples, the superiority in terms of accuracy of the fictitious method over a method consisting in using a staircase approximation of the boundary. We want in this section to illustrate this superiority by an academic case. This section is devoted to a plane wave analysis of a simple problem : a 1-D wave equation with a boundary Dirichlet condition (see Fig. 22).

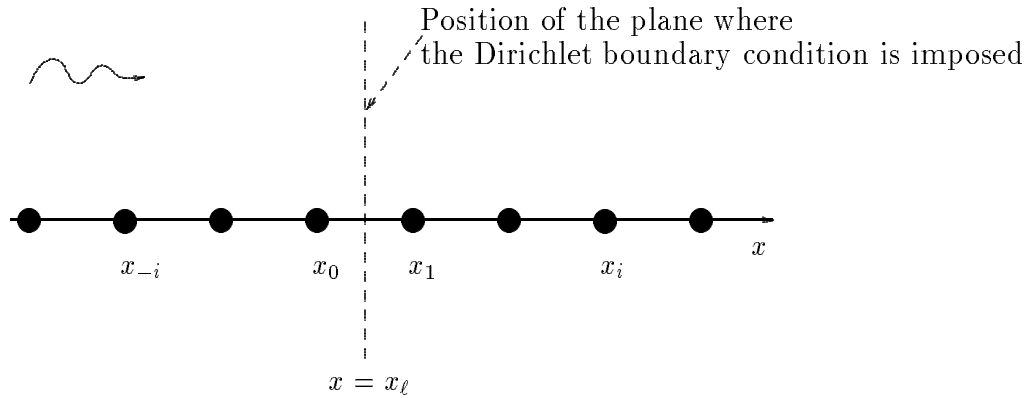


Fig 22: *Geometry of the problem*

More precisely, we consider the problem

$$\begin{cases} \frac{\partial^2 u}{\partial t^2} - \frac{\partial^2 u}{\partial x^2} = 0, & x < x_\ell \\ u(x = x_\ell) = 0. \end{cases} \quad (50)$$

Let  $\Delta t$  and  $h$  to be the time and space steps. We assume that the point  $x_\ell$  is close to the point 0:

$$x_\ell = \ell h, \quad 0 \leq \ell \leq \frac{1}{2}. \quad (51)$$

The classical space and time second order scheme for the staircase approximation is given

by

$$\begin{cases} \frac{u_j^{n+1} - 2u_j^n + u_j^{n-1}}{\Delta t^2} - \frac{u_{j+1}^n - 2u_j^n + u_{j-1}^n}{h^2} = 0, & \forall j \leq -1 \\ u_0^n = 0. \end{cases} \quad (52)$$

In this case (staircase approximation), the point  $x_l$  has been shifted to the point 0.

On the other hand, it is not difficult to write the scheme obtained by the fictitious domain method as

$$\begin{cases} \frac{u_j^{n+1} - 2u_j^n + u_j^{n-1}}{\Delta t^2} - \frac{u_{j+1}^n - 2u_j^n + u_{j-1}^n}{h^2} = \frac{\lambda^n}{h} \left( (1 - \ell)\delta_j^0 + \ell\delta_j^1 \right) & \forall j \\ \ell u_1^n + (1 - \ell)u_0^n = 0. \end{cases} \quad (53)$$

The problem has been extended to the whole space and a Lagrange multiplier  $\lambda$  has been added. Now, let us consider the plane wave solutions.

For the continuous problem (50), an incident plane wave gives rise to a reflected wave and the corresponding solution can be written as

$$\begin{cases} u(x, t) = e^{i\omega t} \left( e^{-ik(x-x_\ell)} + R e^{ik(x-x_\ell)} \right), & x \leq x_\ell \\ \omega = k & \text{(dispersion relation)} \\ R = -1 & \text{(reflection coefficient)}. \end{cases} \quad (54)$$

For the staircase scheme (52), we obtain

$$\begin{cases} u_j^n = e^{i\omega n \Delta t} \left( e^{-ikh(j-\ell)} + R e^{ikh(j-\ell)} \right), & j \leq 0 \\ \frac{2}{\Delta t} \sin \left( \omega \frac{\Delta t}{2} \right) = \frac{2}{h} \sin \left( k \frac{h}{2} \right) & \text{(dispersion relation)} \\ R = -e^{2ikh\ell} & \text{(reflection coefficient)}, \end{cases} \quad (55)$$

while for the fictitious domain scheme (53), the incident plane wave gives rise not only to a reflected wave but also to a transmitted wave inside the fictitious domain. More precisely, the solution we are looking for can be written as

$$\left\{ \begin{array}{l} u_j^n = e^{i\omega n \Delta t} \left( e^{-ikh(j-\ell)} + R e^{ikh(j-\ell)} \right), \quad j \leq 0 \\ u_j^n = e^{i\omega n \Delta t} T e^{-ikh(j-\ell)}, \quad j \geq 1 \\ \lambda^n = e^{i\omega n \Delta t} \hat{\lambda} \\ \frac{2}{\Delta t} \sin \left( \omega \frac{\Delta t}{2} \right) = \frac{2}{h} \sin \left( k \frac{h}{2} \right) \quad (\text{dispersion relation}). \end{array} \right. \quad (56)$$

To find the three unknowns  $R$ ,  $T$  and  $\hat{\lambda}$  in (56), the equations of the scheme associated with the nodes  $j = 0$  and  $j = 1$  as well as the constraint equation are used. The following system is obtained:

$$\left\{ \begin{array}{l} z^\ell + R(1/z)^\ell - Tz^\ell = -\hat{\lambda}h\ell \\ T(1/z)^{(1-\ell)} - ((1/z)^{(1-\ell)} + Rz^{(1-\ell)}) = -\hat{\lambda}h(1-\ell) \\ \ell T(1/z)^{(1-\ell)} + (1-\ell)(z^\ell + R(1/z)^\ell) = 0, \end{array} \right. \quad (57)$$

where  $z$  is given by

$$z = e^{ikh}. \quad (58)$$

Solving (57-58) gives

$$\left\{ \begin{array}{l} \hat{\lambda}h = \frac{(z-z^{-1})(-lz^{\ell-1}-z^\ell+lz^\ell)z}{2\ell-2\ell^2+z-2\ell z+2\ell^2z} \\ R = -\frac{(2z^{2\ell-1}\ell-2z^{2\ell-1}\ell^2+z^{2\ell}-2\ell z^{2\ell}+\ell^2 z^{2\ell}+z^{2\ell-2}\ell^2)z}{2\ell-2\ell^2+z-2\ell z+2\ell^2z} \\ T = \frac{\ell(1-\ell-z^2+lz^2)}{2\ell-2\ell^2+z-2\ell z+2\ell^2z}. \end{array} \right. \quad (59)$$

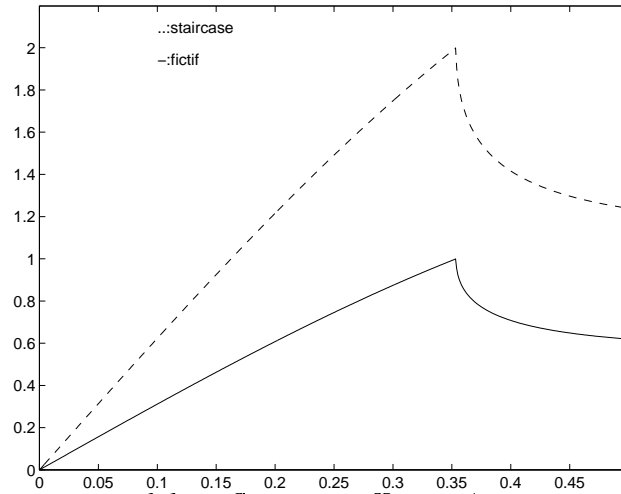


Fig 23: errors of the reflection coefficient (---: staircase and - : fictitious case) versus the inverse of points per wavelength

To compare the two schemes, we define

$$\left\{ \begin{array}{l} \epsilon_{ST} = |R_{staircase} - R_{continuous}| = |z^{2\ell} - 1| \\ \epsilon_{FD} = |R_{fictitious\ domain} - R_{continuous}|. \end{array} \right. \quad (60)$$

A Taylor expansion provides

$$\left\{ \begin{array}{l} \epsilon_{ST} = 2\ell\omega h + O((\omega h)^2) \\ \epsilon_{FD} = 2\ell(1 - \ell)\omega h + O((\omega h)^2). \end{array} \right. \quad (61)$$

As a result, both methods are first order with respect to  $\omega h$ . Note that the transmission coefficient  $T$  is also first order with respect to  $\omega h$ . However, since  $2\ell(1 - \ell) \leq 2\ell$ , the error is smaller for the fictitious domain method than for the staircase approximation method, especially when  $\ell$  approaches  $1/2$ . This is confirmed by the curves of the Figure 23 which compares the errors of the two approaches for different discretizations.

Figure 23 shows the variation of the errors versus the inverse of the number of points per

wavelength. The Courant number  $\Delta t/h$  is  $1/\sqrt{2}$  and the location of the point  $x_\ell$  corresponds to  $h/2$  ( $\ell = 1/2$ ). Although the fictitious method remains first order with respect to the discretization steps, it clearly improves the precision of the reflection coefficient.

**Remark:** It is easy to see that if  $\ell = \frac{1}{2}$ , the reflection coefficient obtained from the fictitious method is one half of the one obtained using the staircase like approximation.

## 6 Conclusion

A fictitious domain method has been introduced for unsteady scattering problems. This method consists in extending the solution inside the object and in introducing an auxiliary variable defined on the boundary. Its main advantage is to permit the use of uniform meshes for the solution. An additional cost is due to the computation of the auxiliary variable. This also imposes a non restrictive compatibility relation between the boundary mesh for the auxiliary unknown and the uniform mesh for the solution. In this paper, we have applied this method for solving time dependent Maxwell's equations. We have tested this algorithm in the 2D case for scattering on a perfect conductor plane. Numerical results show the superiority (in terms of accuracy and memory space) of the fictitious method over the FDTD method. This method may also be extended for solving three dimensional problems where geometrical difficulties result from the intersection of the two meshes ([7]). This fictitious method is applied to solving problems with a Dirichlet condition on the boundary of the obstacle. Moreover, it may be used also for problems with a Neumann condition on the obstacle without any difficulty. But some investigation is necessary to treat other boundary conditions as an impedance condition. This will be the subject of a future work.

## 7 Acknowledgement

We would like to thank Pr. R. Glowinski for helpful comments and suggestions and also S. Garcés for discussions about numerical and theoretical points.

## References

- [1] G.P. Astrakmantev. Methods of fictitious domains for a second order elliptic equation with natural boundary conditions. *U.S.S.R Computational Math.and Math. Phys.*, 18:114–221, 1978.
- [2] C. Atamian, R. Glowinski, J. Periaux, H. Steve, and G. Terrason. Control approach to fictitious domain in electro-magnetism. *Conference sur l'approximation et les methodes numeriques pour la resolution des equations de Maxwell,Hotel Pullmann, Paris*, 1989.
- [3] C. Atamian and P. Joly. An analysis of the method of fictitious domains for the exterior Helmholtz problem. *RAIRO Modél. Math. Anal. Numér*, 27(3):251–288, 1993.
- [4] A. Bendali. *Approximation par elements finis de surface de problemes de diffraction des ondes electro-magnetiques*. PhD thesis, *Université Paris VI* , 1984.
- [5] F. Brezzi. On the existence uniqueness and approximation of saddle-point problems arising from Lagrangian multipliers . *RAIRO Analyse Numérique*, R-2:129–151, 1974.
- [6] G. Cohen, P. Joly, and N. Tordjman. Higher Order Triangular Finite Elements with Mass Lumping for the Wave Equation. *Third International Conference on Mathematical and Numerical Aspects of Wave Propagation*, 1:270–279, 1995.
- [7] F. Collino, S Garcés, P. Joly, and F. Millot. Fictitious domain method for unsteady problems: application to electromagnetic scattering. *International Conference on electromagnetics in advanced applications*, 1995.
- [8] R. Dautray and J.L Lions. *Analyse mathématique et calcul numérique pour les sciences et les techniques*. Masson-Paris, 1988.
- [9] T. Dupont.  $\ell^2$ -estimate for Galerkin methods for second order hyperbolic equations . *SIAM J. Numer. Anal.*, 10(5), 1973.
- [10] B. Engquist and A. Majda. Absorbing boundary conditions for the numerical simulation of

- waves. *Math. of Comp.*, 31:629–651, 1977.
- [11] S.A. Finogenov and Y.A. Kuznetsov. Two stage fictitious components methods for solving the Dirichlet boundary value problem. *Sov. J. Num. Anal. Math. Modelling*, 3:301–323, 1988.
- [12] S. Garcés. *Application des méthodes de domaines fictifs à la modélisation des structures rayonnantes tridimensionnelles Etude mathématique et numérique d'un modèle*. PhD thesis, *Ecole National Supérieure de l'Aeronautique et de l'Espace (Toulouse)*, in preparation.
- [13] V. Girault and R. Glowinski. Error analysis of a fictitious domain method applied to a Dirichlet problem. *Japan J. Indust. Appl. Math.*, 12(3):487–514, 1995.
- [14] R. Glowinski, T.W. Pan, and J. Periaux. A fictitious domain method for Dirichlet problem and applications. *Comp. Meth. in Appl. Mech. and Eng.*, 111:283–303, 1994.
- [15] R. Glowinski, T.W. Pan, and J. Periaux. A fictitious domain method for external incompressible viscous flow modeled by Navier-Stokes equations. *Comp. Meth. Appl. Mech. Eng.*, 112:133–148, 1994.
- [16] G.C. Hsiao and R.E. Kleinmann. Mathematical foundations for error estimation in numerical solutions of integral equations in electromagnetics. *IEEE Trans. Antennas propagat.*, 45(3):316–327, 1997.
- [17] G.I. Marchuk, Y.A. Kuznetsov, and A.M. Matsokin. Fictitious domain and domain decomposition methods. *Sov. J. Num. Anal. Math. Modelling*, 1:3–35, 1986.
- [18] P. Monk. A mixed method for approximating Maxwell's equations. *SIAM J. on Num. Anal. Math. Modelling*, 28:1610–1634, 1991.
- [19] J.C. Nedelec. Mixed finite elements in  $R^3$ . *Num. Math.*, 142:79–95, 1984.
- [20] P.A. Raviart and J.M. Thomas. *Introduction à l'analyse numérique des équations aux dérivées partielles*. Masson, Paris, 1983.
- [21] A. Taflové. *Computational Electrodynamics, The Finite-Difference Time Domain method*. Artech House, London, 1995.
- [22] K.S. Yee. Numerical Solutions of Initial Boundary Value Problems involving Maxwell's Equations in isotropic media. *IEEE trans. on Antennas and Propagation.*, 14:302–307, 1966.

## 7.1 APPENDIX 1: About error estimates

The aim of this appendix is to derive the inequalities (31) of Section 2.4.

We start from the variational equalities satisfied by  $u(t)$  applied to a test function  $v = v_h$  in  $X_h$  ;

$$\frac{d^2}{dt^2}(u, v_h) = -a(u, v_h) + b(v_h, \lambda) \quad \forall v_h \in X_h, \quad (62)$$

or, using  $\epsilon_h(t) = \Pi_h u(t) - u(t)$ ,

$$\frac{d^2}{dt^2}(\Pi_h u, v_h) = -a(u, v_h) + b(v_h, \lambda) - \left( \frac{d^2 \epsilon_h}{dt^2}, v_h \right) \quad \forall v_h \in X_h. \quad (63)$$

The definition of the elliptic projector allows us to replace  $(u, \lambda)$  by  $(\Pi_h u, \Pi_h \lambda)$ , i.e.,

$$\frac{d^2}{dt^2}(\Pi_h u, v_h) + a(\Pi_h u, v_h) - b(v_h, \Pi_h \lambda) = - \left( \frac{d^2 \epsilon_h}{dt^2}, v_h \right). \quad (64)$$

Otherwise,  $u_h$  verifies

$$\frac{d^2}{dt^2}(u_h, v_h) = -a(u_h, v_h) + b(v_h, \lambda_h) \quad \forall v_h \in X_h. \quad (65)$$

Subtracting (65) from (64), and using  $\frac{d^2 \eta_h}{dt^2} \in X$ , (regularity of  $u(t)$  and  $u_h(t)$ ) we obtain

$$\left( \frac{d^2 \eta_h}{dt^2}, v_h \right) + a(\eta_h, v_h) - b(v_h, \tau_h) = - \left( \frac{d^2 \epsilon_h}{dt^2}, v_h \right) \quad \forall v_h \in X_h. \quad (66)$$

Now,  $\eta_h$  is such that

$$b(\eta_h(t), \mu_h) = b(\Pi_h u - u, \mu_h) + b(u, \mu_h) - b(u_h, \mu_h) \quad \forall \mu_h \in M_h, \quad (67)$$

from which we deduce, using the properties of  $\Pi_h$  and the definition of  $u$  and  $u_h$ ,

$$b(\eta_h(t), \mu_h) = b\left(\frac{d^k \eta_h(t)}{dt^k}, \mu_h\right) = 0 \quad \forall \mu_h \in \mathbf{M}_h, k = 1, 2. \quad (68)$$

Let us set  $v_h = \frac{d\eta_h}{dt}$  in (66), we obtain

$$\begin{cases} \frac{d}{dt} \left( \frac{1}{2} E_h(t) \right) - b \left( \frac{d\eta_h}{dt}, \tau_h \right) = \left( \frac{d^2 \varepsilon_h}{dt^2}, \frac{d\eta_h}{dt} \right) \\ E_h(t) = \left| \frac{d\eta_h}{dt} \right|^2 + a(\eta_h, \eta_h), \end{cases} \quad (69)$$

taking  $k = 1$ ,  $\mu_h = \tau_h(t)$  in (68), the  $b$  term vanishes and we get

$$\frac{1}{2} \frac{d}{dt} (E_h(t)) \leq \left| \frac{d^2 \varepsilon_h}{dt^2} \right| \left| \frac{d\eta_h}{dt} \right| \Rightarrow \frac{d}{dt} E_h^{1/2} \leq \left| \frac{d^2 \varepsilon_h}{dt^2} \right|. \quad (70)$$

Using the fact

$$u_h(0) = \Pi_h u(0) \quad \text{and} \quad \frac{du_h}{dt}(0) = \Pi_h \frac{du}{dt}(0), \quad (71)$$

we have

$$\begin{aligned} \sqrt{a(\eta_h, \eta_h)} \quad \text{and} \quad \left| \frac{d\eta_h}{dt} \right| &\leq \int_0^t \frac{dE_h^{1/2}}{ds}(s) ds \leq t \sup_{[0,t]} \left| \frac{d^2 \varepsilon_h}{dt^2} \right|. \\ |\eta_h(t)| &\leq \int_0^t E_h^{1/2}(s) ds \leq \int_0^t \int_0^s \left| \frac{d^2 \varepsilon_h}{dt^2} \right| ds dt \leq \frac{t^2}{2} \sup_{[0,t]} \left| \frac{d^2 \varepsilon_h}{dt^2} \right| \end{aligned} \quad (72)$$

therefore

$$\|\eta_h\|_{\mathbf{X}} = \sqrt{|\eta_h|^2 + a(\eta_h, \eta_h)} \leq \left( \frac{t^2}{2} + t \right) \sup_{[0,t]} \left| \frac{d^2 \varepsilon_h}{dt^2} \right|. \quad (73)$$

We have obtained the inequality (31) for the error  $\eta_h$ . To get the second inequality, we start from the inf-sup condition

$$\|\tau_h(t)\|_{\mathbf{M}} \leq \frac{1}{C'} \sup_{v_h \in \mathbf{X}_h} \frac{b(v_h, \tau_h)}{\|v_h\|_{\mathbf{X}}}, \quad (74)$$

and we use both equation (66) and the continuity of the bilinear form  $a$  to get

$$\begin{aligned}
|b(v_h, \tau_h)| &\leq \left| \left( \frac{d^2 \eta_h(t)}{dt^2}, v_h \right) \right| + |a(\eta_h(t), v_h)| + \left| \left( \frac{d^2 \varepsilon_h}{dt^2}, v_h \right) \right| \\
&\leq M \|\eta_h\|_{\mathbf{X}} \|v_h\|_{\mathbf{X}} + \left( \left| \frac{d^2 \eta_h}{dt^2} \right| + \left| \frac{d^2 \varepsilon_h}{dt^2} \right| \right) |v_h| \quad \forall v_h \in \mathbf{X}_h.
\end{aligned} \tag{75}$$

Until now, we have only used the  $C^2$  regularity of the solution. In order to bound the H-norm of  $\frac{d^2 \eta_h}{dt^2}$ , we need  $C^3$  regularity. Indeed, in this case, all of the previous calculations can be rewritten for the derivatives of the functions. In particular, we have

$$\left| \frac{d^2 \eta_h}{dt^2} \right| \leq t \sup_{[0,t]} \left| \frac{d^3 \varepsilon_h}{dt^3} \right|.$$

Finally, combining the different results provides us with

$$\begin{aligned}
C' \|\tau_h(t)\|_{\mathbf{M}} &\leq \left( M \|\eta_h\|_{\mathbf{X}} + t \sup_{[0,t]} \left| \frac{d^3 \varepsilon_h}{dt^3} \right| + \left| \frac{d^2 \varepsilon_h}{dt^2} \right| \right) \\
&\leq \left( M \left( \frac{t^2}{2} + t \right) + 1 \right) \sup_{s \in [0,t]} \left| \frac{d^2 \varepsilon_h}{dt^2} \right| + t \sup_{s \in [0,t]} \left| \frac{d^3 \varepsilon_h}{dt^3} \right|,
\end{aligned}$$

and the proof is achieved.